ACS Catalysis

Research Article

Cite This: ACS Catal. 2018, 8, 3365–3375

pubs.acs.org/acscatalysis

Surface Activation of Transition Metal Nanoparticles for Heterogeneous Catalysis: What We Can Learn from Molecular Dynamics

Xingchen Liu,[†,‡,§] Xiaodong Wen,*[,†,‡] and Roald Hoffmann*[,§]

[†]State Key Laboratory of Coal Conversion, Institute of Coal Chemistry, Chinese Academy of Sciences, Taiyuan 030001, China

[‡]National Energy Center for Coal to Liquids, Synfuels CHINA Co., Ltd, Huairou District, Beijing 101400, China

[§]Department of Chemistry and Chemical Biology, Cornell University, Baker Laboratory, Ithaca, New York 14853-1301, United States

Supporting Information

ABSTRACT: Many heterogeneous reactions catalyzed by nanoparticles occur at relatively high temperatures, which may modulate the surface morphology of nanoparticles during reaction. Inspired by the discovery of dynamic formation of active sites on gold nanoparticles, we explore theoretically the nature of the highly mobile atoms on the surface of nanoparticles of various sizes for 11 transition metals. Using molecular dynamics simulations, on a 3 nm Fe nanoparticle as an example, the effect of surface premelting and overall melting on the structure and physical properties of the nanoparticles is analyzed. When the nanoparticle is heated up, the atoms in the outer shell appear amorphous already at 900 K. Surface premelting is reached at 1050 K, with more than three liquid atoms, based on the Lindemann criterion. The activated atoms may transfer their extra kinetic energy to the rest of the nanoparticle and activate other atoms. The dynamic studies indicate that the number of highly mobile atoms on the surface increases with temperature. Those atoms with a high Lindemann index, usually located on the edges or vertices, attain much higher kinetic energy than other atoms and potentially form different active sites in situ. When the temperature passes the surface premelting temperature, a drastic change in the coordination number (SCN) of the surface atoms occurs, with attendant dramatic broadening of the distribution of the SCN, suppling active sites with more diverse atomic coordination numbers. The electronic density of states of a nanoparticle tends to "equalize", due to the breaking of the translational symmetry of the atoms in the nanoparticle, and the d-band center of the nanoparticle moves further away from the Fermi level as the temperature increases. Besides Au, other nanoparticles of the transition metals, such as Pt, Pd, and Ag, may also have active sites easily formed in situ.

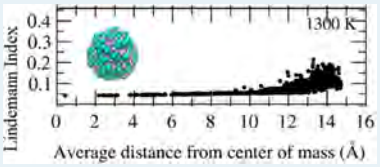

KEYWORDS: *nanoparticles, surface premelting, metal clusters, catalysis, molecular dynamics*

INTRODUCTION

For some time it has been known that the melting point of a metal changes inversely with particle dimensions.[1] Thus, nanoparticles have a substantially lower melting point than their bulk form. Because of their low coordination number and the greater degree of freedom in their motions, surface atoms have higher mobility than atoms in the bulk. The latter fact makes the melting temperature of the surface atoms even lower than that of the core atoms of a nanoparticle, causing the phenomenon of surface melting, or "surface premelting", as designated by Bachels,[2] or "dynamic coexistence melting", by Alavi et al.[3] From extensive studies of phase transitions in small clusters, Berry et al.[4] concluded that there exists a finite range of temperatures over which solidlike and liquidlike clusters can coexist in equilibrium. A very interesting case[5] of phase coexistence in nanoparticles is that of gallium, with coexistence of melted surfaces and solid core over a broad range of temperature from 180 to 800 K. The materials were reported as "neither solid nor liquid".[6] Other earlier examples confirmed by experiments are Sn,[2,7] Pb,[8] and Pt.[9]

In heterogeneous catalysis, the catalysts prepared are usually characterized at low-temperature and with inert gas protection, after synthesis by various spectroscopic and microscopic tools. Such characterization usually assumes that the structures of the catalysts do not change, and the structural features observed in the characterization remain fixed during reaction. This assumption is usually true in low temperature electro-catalysis and photocatalysis. However, in many thermally driven industrial heterogeneous catalysis reactions, where highly dispersed nanoscale catalysts are involved, this assumption may not be valid, and the morphology and the arrangement of atoms on the surfaces may change at high temperature.

Such changes in the microscopic properties of nanoparticles with temperature have been well-recognized in the physics and material science community and studied extensively over the past few decades. After reviewing[10] the experimental and theoretical studies of metal clusters up to the 1990's, de Heer pointed out that the dynamic properties of metallic nanoclusters may deviate from the standard "shell-model" description of metallic nanoparticles. Using optical spectropho-

Received: December 27, 2017
Revised: March 3, 2018
Published: March 9, 2018

DOI: 10.1021/acscatal.7b04468
ACS Catal. 2018, 8, 3365–3375

tometry, Kirkland et al. observed the evolution of colloidal metal nanoparticles in solution.[11] Dislocation generation in nanocrystals was studied by Penn and Banfield.[12] The role of strong metal−support interactions (SMSI) on the structure and dynamics of nanoparticles have been widely studied experimentally; here we cite only a few relevant references.[13,14] On the basis of X-ray absorption fine structure (EXAFS) studies, the atomic scale ordering of supported metal nanoparticles was explained by Frenkel et al. using surface atom bond relaxation arguments.[15] The elastic driven surface instabilities of nanoparticles have been discussed by Müller and Saúl, focusing on the relevant thermodynamics and kinetics.[16] The stabilization of nanoparticles by defects, steps, kinks, and external modifications is discussed in terms of internal strain by Mayoral et al.[17] The metamorphosis of Au@Fe_2O_3 nanoparticles at high temperature was explored with in situ electron microscopy and X-ray diffraction, with a fluidlike fusion of Au and Fe_2O_3 nanoparticles at a temperature far below their size-reduced melting points.[18]

Theoretical modeling has also contributed a great deal to the understanding of the structural evolution of nanoparticles, including the solid−liquid phase behavior in microclusters,[4] the existence of a quasi-melting regime in small particles,[19] the liquid skin nucleation model of melting,[20] the role of bond order deficiency on the size-dependent melting of nanoparticles,[21] the amorphization of nanoparticles,[22,23] their melting and freezing,[24−27] and their morphological transitions.[28−30] For more information on these aspects, the reader may refer to the review articles of Baletto,[31] Barnard,[32] and Marks.[33]

On the basis of the fundamental studies by physicists and material scientists cited by us, in the past decade, the surface structure evolution of nanoparticles has attracted the attention of scientists working directly on catalysis. Using X-ray scattering methods, rapid changes of the shape of silver nanoparticles at room temperature upon exposure to the reactants were discovered, followed by complex evolution of shape with increasing temperature.[34] Using molecular dynamic simulations, Zhang et al. studied the size-dependent stability of step-edge surface sites on cobalt nanoparticles.[35] The shape evolution of supported Pt nanoparticles was studied experimentally for CO, NH_3, formic acid oxidation,[36] and NO oxidation,[37] and theoretically by Barron et al.[38]

In catalysis, surface melting will certainly not only change the surface morphology of the nanoparticles but also naturally affect the topology of the active sites, as well as the surface diffusion and surface reactions on them. We also may not only be interested in the situation where all surface atoms melt. As long as there are some atoms that have high mobility, they could potentially affect the catalytic activity of the entire nanoparticle, and this could be generally referred to as surface activation. For example, using ab initio molecular dynamics (AIMD), a single-atom catalytic active site (to catalyze carbon monoxide oxidation) was found by Li and Rousseau et al. to be dynamically created on Au_{20} nanoparticles supported on CeO_2 (111) at 700 K and to disappear after the reaction.[39] Using the same method, they also discovered the evolution of active sites and morphology of supported nanoparticles of Au/TiO_2 for CO oxidation.[40,41] Similar studies were used to find the equilibrium structure of the carbon and alumina-supported Co/La_2O_3 for alcohol synthesis from syngas[42] and $MgAl_2O_4$-supported Rh and Ir catalysts for methane steam reforming.[43] Dynamically formed single atom sites were not found in this work. We may wonder if the dynamical formation of single-atom active sites is a unique feature of the Au nanoparticle or something that may happen for all transition metals. To provide greater insight into these phenomenon, in situ techniques are being developed in nanoscale heterogeneous catalysis to overcome the restriction of static experimental methods and follow the dynamic evolution of the catalytic system in real time.[44−50] However, due to their complex physical-chemical properties at the nanometer scale, even the location of the active site in working conditions often remains uncertain.[51]

In addition, many important industrial heterogeneous reactions happen at relatively high temperature, where dynamic effects are significant. For example, the activation of methane, the most abundant hydrocarbon on earth, to produce syngas,[52] requires 700−1100 °C on Co, Ru, Ni, Rh, and Cu catalysts. The oxidation of ammonia for nitric acid production[53] is conducted optimally at 810−940 °C with a Pt catalyst, depending on the pressure and NH_3 volume ratio. Other examples include solid oxide fuel cells[54] (500−1000 °C on Ni), carbon nanotube formation[55] (750 °C on Fe), and the synthesis of hydrocyanic acid from ammonia and methane[56] (1200 °C on Pt). Moreover, since the reactions take place at the interfaces between the gas and the solid phase, for strong exothermic reactions such as Fischer−Tropsch and Haber-Bosch processes, much reaction heat is released at the interface (i.e., the catalyst surface). Then the temperature of the catalyst surface may grow to exceed that in the impinging gas phase by as much as a few hundred degrees, due to the poor thermal conductivities of gases.[57] The surface melting of the nanocatalysts may be enhanced thereby. Recently, Losurdo et al.[5] reported the observation of solid-core/liquid-shell coexisting gallium nanoparticles (with potential catalytic application) of about 50 nm in size, deposited on a sapphire substrate, which has a coexistence temperature window of more than 600 K. Moreover, the recent discovery[58] of highly active nanoscale liquid metal catalysts increased the interest in understanding the interaction between melted nanoparticle surfaces and molecules.

Despite the importance of surface melting and activation of nanocatalysts in heterogeneous catalysis, their effect on the catalytic activity of the nanoparticles is still not well-understood. There is some theoretical work on the surface melting of Fe,[59] Ni,[60] Cu,[61] Ag,[62,63] and Cu−Ag bimetallic[64] nanoparticles. However, none of these contributions discuss the relationship of surface melting/activation to heterogeneous catalysis. In this paper, we report a systematic study of the surface activation of nanoparticles of 11 transition metal elements that are commonly used for catalysis (Fe, Co, Ni, Cu, Mo, Ru, Rh, Pd, Ag, Pt, and Au). The goal of this work is to provide atomistic and conceptual understanding of the surface activation and premelting phenomenon of transition metal particles and to shed light on their potential effects on heterogeneous catalysis.

Since surface premelting can only happen in nanoparticles (not microparticles or the bulk), where the surface tensions of solid−liquid, liquid−vapor, and solid−vapor obey the inequality $\gamma_{sv} > \gamma_{sl} + \gamma_{lv}$ (γ_{sv}, γ_{sl}, and γ_{lv} represent the surface tension between solid−vapor, solid−liquid, and liquid−vapor, respectively),[1] we restrict our study to nanoparticles of the transition metals with diameters of 1 to 8 nm. By analyzing the Lindemann index for the nanoparticles from molecular dynamic (MD) trajectories, trends in surface melting for the transition metals are elucidated. The connection between the activation of

DOI: 10.1021/acscatal.7b04468
ACS Catal. 2018, 8, 3365−3375

the surface atoms in surface melting and the catalytic performance of the nanocatalysts is in this paper discussed conceptually. In future work, we will explore some specific catalytic reactions.

COMPUTATIONAL METHOD

The Lindemann index[65] is the quotient of the root-mean-square distance of an atom from its equilibrium position to the averaged nearest neighbor distance of that particular atom. It measures roughly the vibrational motion of atoms and can be calculated as a function of interatomic distance. The index is defined as

$$\delta_i = \frac{1}{N-1}\sum_{j\neq i}\frac{\sqrt{\langle r_{ij}^2\rangle_T - \langle r_{ij}\rangle_T^2}}{\langle r_{ij}\rangle_T} \quad (1)$$

$$\delta = \frac{1}{N}\sum_i \delta_i \quad (2)$$

where δ_i and δ are the Lindemann indices of the ith atom and the cluster, respectively, N is the number of atoms, r_{ij} is the interatomic distance between atoms i and j, and $\langle\cdots\rangle_T$ denotes the thermal average at temperature T. A high Lindemann index naturally indicates high vibrational motion of the particular atoms which make up the active sites. The melting point may be seen as the temperature at which the Lindemann index increases suddenly.[66,67] It is generally accepted that values of δ below 0.1 indicate an ordered solid state, and a value above 0.1 points to a liquid. This is known as the Lindemann criterion for melting.[1,65] In accordance with the model developed by Chernyshev,[68] strict surface premelting only takes place if the NP radius is larger than a critical radius, which is different for different materials. And the surface melting temperature in Chernyshev's model can be calculated as a function of the melting point.

In catalysis, we are not necessarily interested in the situation where all of the surface atoms melt, and a core−shell type liquid−solid interface emerges, reaching the "surface premelting" regime defined by Chernyshev. Rather, we believe that of more relevance is the situation where some of the surface atoms gain high mobility, sufficient to affect catalytic reactions on these surface atoms. Following the Lindemann criterion, the surface premelting temperature is defined as the temperature where a certain fraction of atoms have δ larger than 0.1. To rule out error caused by random events where only a particular atom obtains high kinetic energy, the surface premelting temperature is defined arbitrarily as the temperature with at least three atoms with δ larger than 0.1.

We are interested in nanoparticles with sizes of 1−10 nm, because it is in this range that metal nanoparticles undergo a transition from atomic to metallic properties. For this reason, five sizes are chosen (roughly 1, 2, 3, 4, 6, and 8 nm) to build nanoparticles with the Wulff construction[69] for the transition metal elements studied. The surface energy data behind the Wulff construction derives from the literature (BCC:[70] Fe, Mo; FCC:[71] Rh, Ni, Pd, Pt, Cu, Ag, Au; and HCP: Ru, Co[72]). The shape of the largest nanoparticle of the elements is shown in Figure 1; detailed information about the nanoparticles constructed is provided in the Supporting Information.

The MD simulations are performed with the LAMMPS code using the EAM potentials (Foiles et al:[73] Au, Ag, Cu, Ni, Pd, and Pt; Pun et al:[74] Co; Mendelev et al:[75] Fe; Fortini et al:[76] Ru; and Sheng et al:[77] Rh) that have been previously published, and which lead to realistic bulk melting point or sublimation energy. It also has been shown that modeling of the melting behavior of gold nanorods using the EAM potential[78] agrees with laser heating experiments.[79] For Mo, for which a reliable EAM potential is not available, the N-Body semiempirical potential by Ackland and Thetford[80] was used. The electronic structure calculation was done at the density functional tight-binding (DFTB) level of theory with the DFTB+ code,[81] with published parameters.[82]

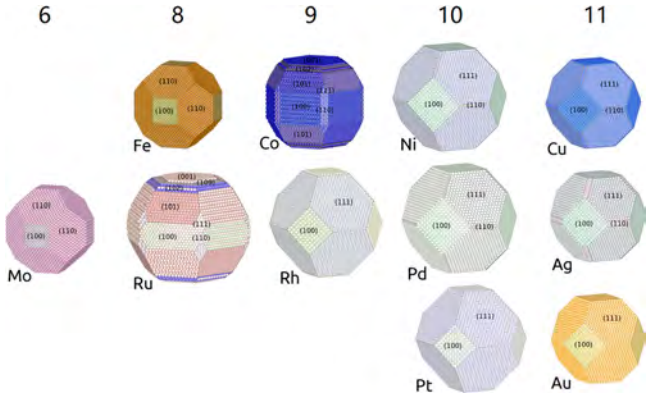

Figure 1. Investigated structures of the transition metal nanoparticles from a Wulff construction.

RESULTS AND DISCUSSION

Melting and Surface Premelting Temperature of Fe Nanoparticles. Because of the large amount of data collected, we will use Fe, in most cases a 3 nm Fe_{1075} nanoparticle, as an example for the discussion. Figure 2a shows the overall Lindemann index and the potential energy of the Fe_{1075} (3 nm) nanoparticle. From these curves, the melting point can be deduced as ∼1350 K. It is clear that the melting point from the Lindemann index criterion is consistent with that derived from the potential energy criterion. However, the Lindemann index is a more explicit and sharper indicator of the melting point. Both diagrams suggest the existence of a first-order phase transition in the nanoparticle at about 1350 K, accompanied by evolution of latent heat. Since the Lindemann index is a measurement of the vibrational motion of the atoms, it is also a good indicator of the entropy change during heating. Clearly, much of the latent heat absorbed by the nanoparticle is contributed to the increase in entropy.

The dependence of melting and surface premelting temperature of an Fe nanoparticle on the size of the cluster is shown in Figure 2b, aiming for a quantitative understanding of their relation. When the Fe nanoparticle is large, its surface activation temperature (as defined earlier) is 500 K less than the complete melting temperature of the nanoparticle. As the size of the nanoparticle decreases (the $1/R_m$ value increases), the difference between the surface activation temperature and the complete melting temperature becomes smaller and is about 200 K in the case of Fe nanoparticles. However, the ratio of the two is maintained at about 0.75, regardless of the particle size. This can be used as a rule-of-thumb to estimate the surface activation temperature of nanoparticles from their complete melting temperature. The bulk melting temperature of Fe calculated using the same potential is 1772 K,[75] and the experimental melting temperature of Fe is 1812 K.

DOI: 10.1021/acscatal.7b04468
ACS Catal. 2018, 8, 3365−3375

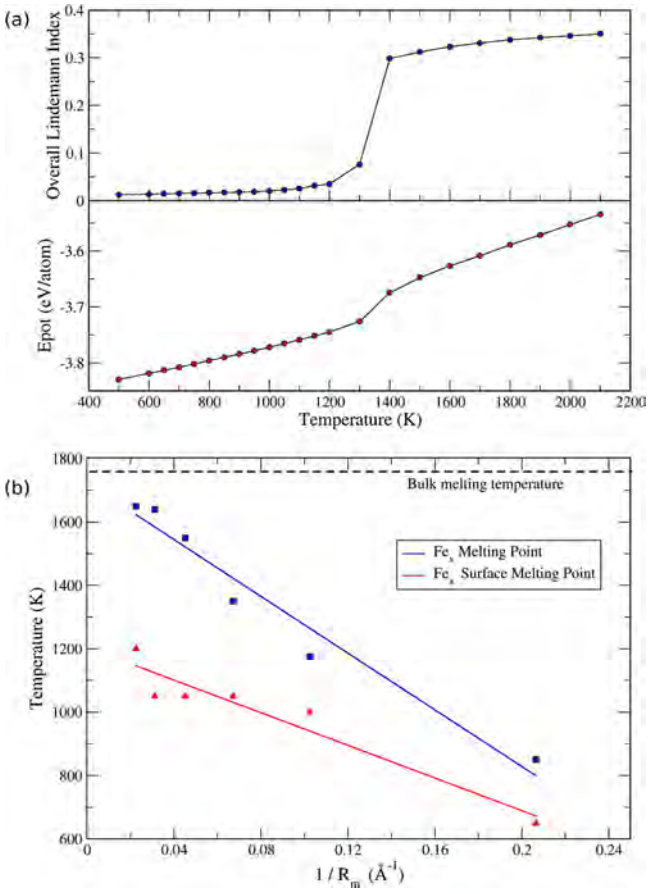

Figure 2. (a) Calculated Lindemann index and potential energy curve of the Fe_{1075} (3 nm) Wulff nanoparticle. (b) Melting point and surface premelting (surface activation) point of different sizes of Fe nanoparticles.

Surface Premelting and the Highly Mobile Atoms on the Surface. Figure 3 shows the radial distribution of the Lindemann indices at different temperatures for all atoms in the 3 nm Fe_{1075} nanoparticle, averaged over the trajectories of the MD simulations. As expected, not much happens at low temperatures. Up to 800 K, the atoms remain pretty much in their crystalline positions. Starting from 1000 K, some of the surface atoms have a large amplitude of movement from their original lattice positions. The atoms that are activated are mostly located on the edges of the Wulff-shape nanoparticle. At 1000 K, two of the surface atoms may be identified as liquid state atoms by the Lindemann criterion. These atoms have high mobility and are likely to be involved in the dynamic formation of active sites on the nanoparticle, similar to the case of dynamic formation of single-atom active sites on Au_{20}/CeO_2 at 700 K reported in literature. When the temperature is increased further, surface melting becomes more significant, illustrated by the increase in the number of surface atoms that have high mobility. Surface activation, defined as three atoms having a Lindeman index ≥ 0.1, is reached at 1050 K. These atoms, with high kinetic energy, are mobile on the surface.

How does an activated atom move on the nanoparticle? Figure 4 tracks the movement of one such activated atom at

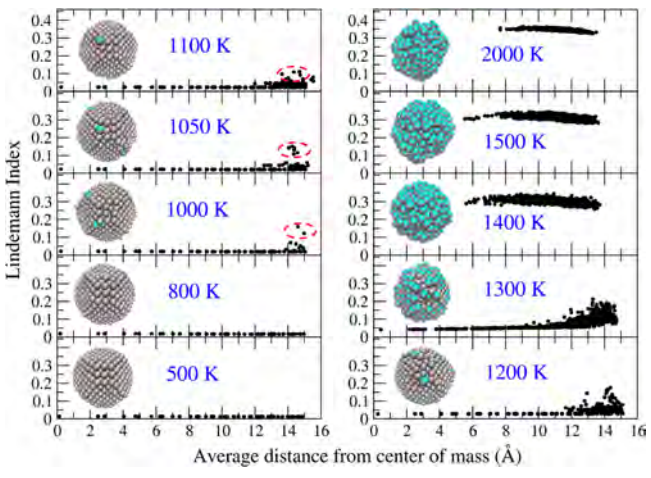

Figure 3. Calculated Lindemann index (each point in the plots represent an atom) of the atoms in a 3 nm Fe_{1075} nanoparticle as they vary with the distance of the atom from center of mass of a particle at different temperatures. Atomic configurations taken from a snapshot of the MD at all the temperatures are embedded in the corresponding plots. The Fe atoms are represented by spheres; solid atoms ($0 < \delta_i < 0.1$) are gray balls and liquid atoms ($\delta_i > 0.1$) are cyan balls.

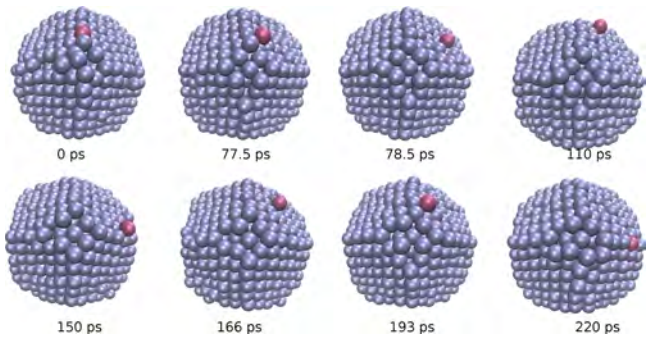

Figure 4. Dynamic relocation of an activated surface Fe atom (in red color, ID: 373) on the nanoparticle from an equilibration trajectory at 1050 K, starting from 0 ps.

1050 K. In the beginning, the atom is located on the edge of the particle. It then moves to the top of a flat surface, forming a "single-atom" site. Afterward, it moves to another edge of the particle, filling the vacancy due to the leaving of another activated atom. Because of the high mobility of these atoms, when a support is supplied, we can imagine that these atoms may temporarily "flow" from the rest of the nanoparticle to the support, forming supported "single-atom" type active sites.

At 1000, 1050, and 1100 K, although the activated Fe atoms are all edge atoms, they are not identical. The extra kinetic energy of one active atom can be transferred to another atom on the surface, not necessarily nearby, by the complex vibrations of the nanoparticle. This is in agreement with the findings of Engelmann,[60] who suggests that because of the small size of the cluster, fluctuations in a small part of the cluster will immediately affect the rest of the cluster. Therefore, the classical way of separating solid and liquid phases in space has little meaning at nanoscale. Rather, the physical state of the cluster might change as a function of time, so that there is a dual-state system in time. At 1300 K, where most of the surface atoms have melted, the Fe atoms in the core of the nanoparticle still remain in their lattice positions, maintaining a crystalline core. At 1400 K, complete melting of the nanoparticle is observed.

DOI: 10.1021/acscatal.7b04468
ACS Catal. 2018, 8, 3365−3375

An interesting observation in Figure 3 is the formation of seemingly "hollow shells" at high temperature, when complete melting is reached. At temperatures above 1400 K on average, none of the atoms seem to remain in the core regions, with average distance smaller than 5 Å from the center of mass of the nanoparticle. To further examine this phenomenon, a slice of space was defined (-1.2 Å $< x <$ 1.2 Å), and the atoms that come into the slice with time are shown in Figure 5. From these

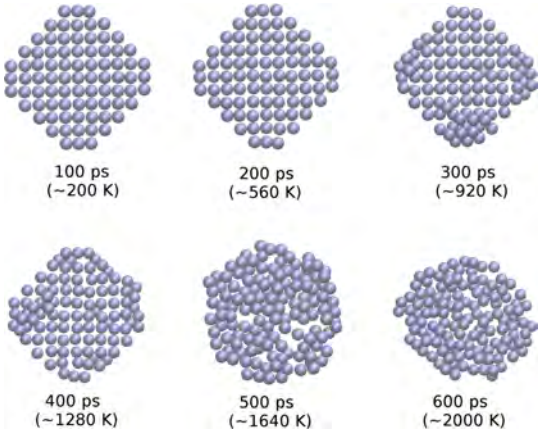

Figure 5. Fe atoms that appears in a slice of space during the heating of a 3 nm Fe_{1075} nanoparticle. The instant temperature of the system at the corresponding simulation time is provided underneath.

snapshots, no hollow region was detected even at 2000 K. This makes us reconsider the idea of hollow shells in Figure 3. These apparent hollow shells at the higher temperature of the simulation do not mean that there are no atoms in the core region but rather imply that statistically no atoms remain in the core region over a long period of time. Instead, these atoms move quickly through the core. The core (with, say, half of the radius of the particle) constitutes only a small fraction (about 1/8) of the entire volume of the nanoparticle, and the shell makes up most of the volume (about 7/8).

For melted nanoparticles in a liquid state, the atoms can move freely over the entire volume of the nanoparticle, and the average distance of the atom to the center of mass is weighted much higher in the shell region than the core region, causing the average distance to the center of mass to be larger than radius of the core (about 5 Å in this case). After melting, the higher the temperature, the more degrees of freedom are available to the Fe atoms in motion. So the distribution of the average distance of an Fe atom from the center of the nanoparticle would become more compact, centered around the distance-of-half-volume ($d_{1/2v}$) of the particle, about 11.9 Å. In the extreme of an ideal gas, we could expect the average distance from the center of mass estimated in this way to form a sphere at $d_{1/2v}$, if we set up an external spherical potential of radius 15 Å to prevent the gasification of the melted nanoparticle.

Phase Diagram of the Melting Fe Nanoparticle. To calculate of the liquid fractions of the whole system quantitatively and thermodynamically, we apply the equilibrium constant scheme of Engelmann[60] (Figure 6a). For an isothermal process which starts from the solid state, the transition to the equilibrium state of a certain temperature with liquid fraction y and solid fraction x has an energy of ΔU, as is shown in Figure 5a. Since in our simulations, the external

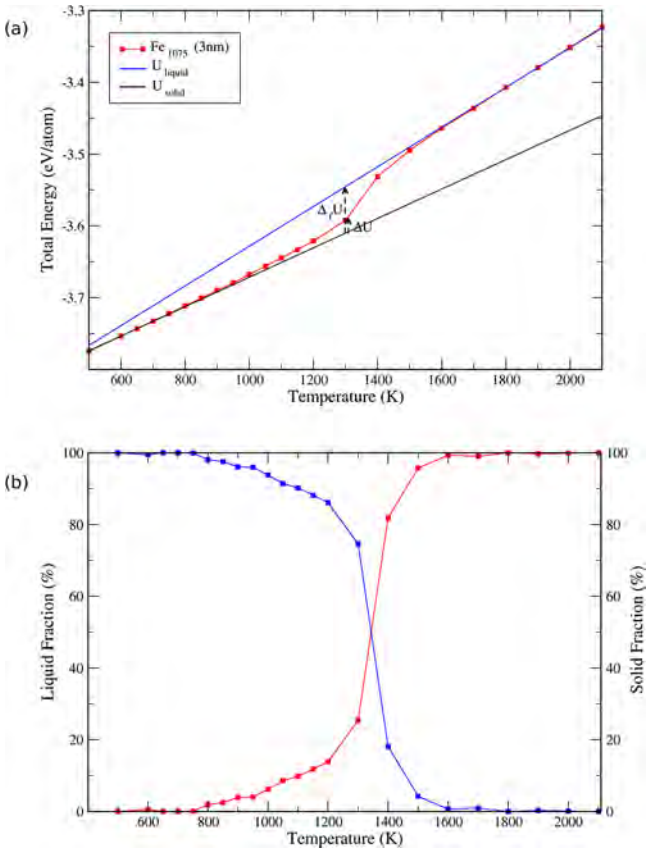

Figure 6. (a) Time-averaged total energy curve of the Fe_{1075} nanoparticle at different temperatures; the lower black line indicates the variation in the total energy of the solid cluster with temperature, and the higher blue line shows how the total energy of the liquid cluster varies with temperature. (b) Calculated liquid fraction (red curve) and solid fraction (blue curve) of the 3 nm Fe_{1075} nanoparticle, based on a total energy graph from the scheme of Engelmann et al.[60]

pressure is zero, the Gibbs free energy will be zero at equilibrium:

$$\Delta G = \Delta H - T\Delta S = 0$$

H equals $U + pV$, and at zero temperature, H equals U. ΔS is the difference in entropy between the solid state (initial) and the solid/liquid mixed state (final): $\Delta S = \int_i^f \delta Q/T$. Since only a small fraction of y melts and the system is in isobaric condition, the difference in entropy can be approximated as $y\Delta_f H/T$, where $\Delta_f H$ is the enthalpy of fusion of the whole system, equivalent to the internal energy of fusion $\Delta_f U$ (Figure 5a) in isobaric conditions. This leads to

$$\Delta G = \Delta U - T\frac{y\Delta_f U}{T} = 0$$

From this equation, the liquid fraction y can be calculated as

$$y = \frac{\Delta U}{\Delta_f U}$$

Here, ΔU (Figure 6a) is the change of internal energy from solid state to the equilibrium mixture of solid and liquid state during surface premelting.

The liquid and solid fractions in the 3 nm Fe_{1075} nanoparticle are presented in Figure 6b. Surface premelting becomes noticeable at about 900 K, where the liquid fraction reaches

DOI: 10.1021/acscatal.7b04468
ACS Catal. 2018, 8, 3365−3375

5%. This is in agreement with the observation of liquid atoms at 1000 K from the Lindemann criterion in Figure 3.

In the above sections, we have discussed the possibility of in situ formation of active sites on nanoparticles due to surface premelting. These dynamically formed new active sites may or may not be the dominant factor in determining the catalytic activity of a nanoparticle. On the basis of the case of an Au nanoparticle supported on CeO_2 (for CO oxidation) reported in literature,[39] we expect that when nanoparticles are supported, the activated atoms characterized by high Lindemann indexes could form highly active "single-atom sites" on the support. And these in turn might greatly affect the catalytic activity of the nanoparticle. However, we cannot be certain if these activated atoms on the nanoparticle, dynamically forming "add-atom" sites, would be decisive in determining the catalytic activity of the nanoparticle. We intend to study this in future work.

No matter how active these in situ formed sites are, a Lindemann index criterion can only characterize the mobile atoms and the dynamically formed active sites. It does not recognize intrinsic active sites that have high catalytic activity but do not involve mobile atoms or the dynamic site formation. Consequently, a more general indicator is needed to discuss the effect of surface premelting on the catalytic activity of a nanoparticle. And for that purpose, we proceed to explore the coordination number of surface atoms.

Surface Premelting of an Fe Nanoparticle and Its Potential Catalytic Activity: Coordination Number. It is known that even slight changes in the surface structure of catalytic materials can have great impact on their activity and selectivity.[83] It has been shown by Calle-Vallejo et al.[84] that a volcano-shaped activity-coordination relationship exists and that the catalytic activity of the nanoparticles is closely related to the number of the nearest neighbors of the surface atoms on the nanoparticle. We therefore wished to explore the effect of surface premelting on the coordination number of surface atoms. In this work, the surface atoms are defined using a spider algorithm,[38] which requires that for any atom to be labeled as a surface atom, there can be at least one additional atom of the same type that can fit onto the top and in contact with the surface atom. To be specific, for each atom, 5000 random points are created on a sphere with radius of d_{min} = 2.46 Å, which is nearest Fe−Fe distance in Fe BCC lattice. If an atom is a surface atom then there is at least one point among the trial random points, for which the minimum distance to all of the rest of the atoms in the nanoparticle is d, for in that case an additional Fe atom can be fitted. This is schematically shown in Scheme 1.

Coordination numbers of the surface atoms (SCN) are determined using the radial distribution function. For liquids, there are at least four ways to compute the CN from the radial distribution function $g(r)$: symmetrizing the first peak in $rg(r)$; symmetrizing the first peak in $r^2g(r)$; decomposition of $r^2g(r)$ into shells; and computation of area to the first minimum in $r^2g(r)$, as discussed by Mikolaj and Ping[85] and also by Wen et al.[86] Different method may lead to different CNs. In this work, the coordination number is calculated with the fourth method: integration to the first minimum in $4\pi r^2\varphi g(r)$. The radial pair distribution function $g(r)$ among all the Fe atoms in the Fe nanoparticle at different temperatures is shown in Figure 7. To be consistent in the choice of the cutoff radius for solid and liquid state, we use the first minimum of the radial distribution function (i.e., 3.5 Å) as the cutoff distance. From the MD trajectories, the SCN of each atom is calculated by integrating its radial distribution function to the cutoff distance of 3.5 Å.

Scheme 1. Surface Atom Spider Criterion[a]

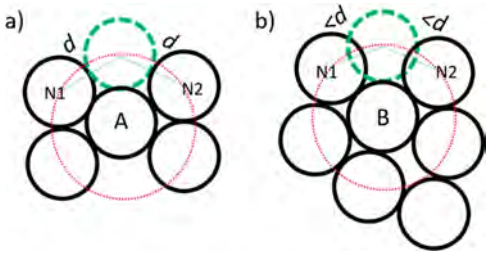

[a]The atom A in (a) is a surface atom because a new atom (green sphere with dashed lines) can fit into the space around it. Atom B in (b) is not a surface atom because a new atom (green sphere with dashed lines) cannot fit on top of B as a result of the steric constraints from its neighbors N1 and N2.

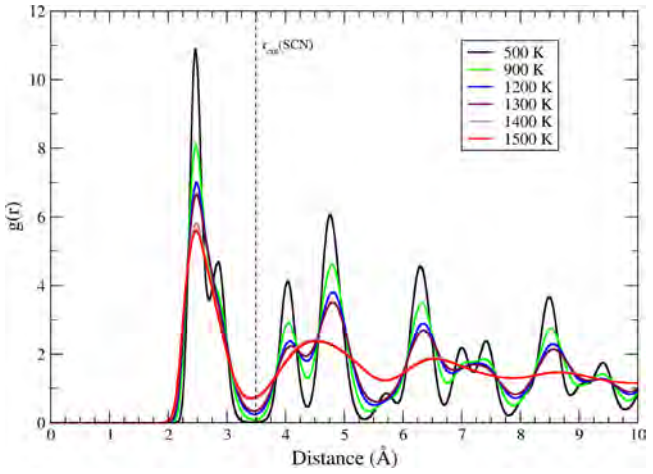

Figure 7. Radial pair distribution function of the 3 nm Fe_{1075} nanoparticle at different temperatures.

With the above definition of SCN, Figure 8 shows the distribution of the SCN for the Fe atoms at various temperatures. At 500 K, there are six bins of SCN, with bin size of 0.5. The highest column at 10 corresponds to the atoms on the (110) facets, the second highest at 14 corresponds to the atoms at (100) facets; the others belongs to atoms at the edges and vertexes of the nanoparticle. That the SCN of the surface atoms is higher than the coordination of a BCC lattice, namely 8, occurs because we used the liquid state cutoff distance 3.5 Å in the radial distribution function to calculate CN. And while we usually think of 12 as the highest (close-packed) CN, in fact in a bcc lattice the CN is effectively 14 (8 + 6), given the slightly higher tolerance or cutoff in distance.

At 800 K, as the nanoparticle approaches surface premelting and a small fraction of the atoms are in liquid state (see Figure 6b), the SCN of the atoms on the (100) and (110) facets does not change much, but the atom at one of the edges changes slightly from 8 to 8.5. At 1200 K, when the temperature passes the surface premelting temperature, there is a drastic change in the SCN of the surface atoms. The number of surface atoms on the (110) and (100) with SCN of 14 and 10 drops substantially, and a broad peak appears at 7.5−10 neighbors. Also, atoms with SCN between 10 and 14 appear, although with relatively small numbers. At 1400 K, when the system passes the melting temperature, the melting of the core region

DOI: 10.1021/acscatal.7b04468
ACS Catal. 2018, 8, 3365−3375

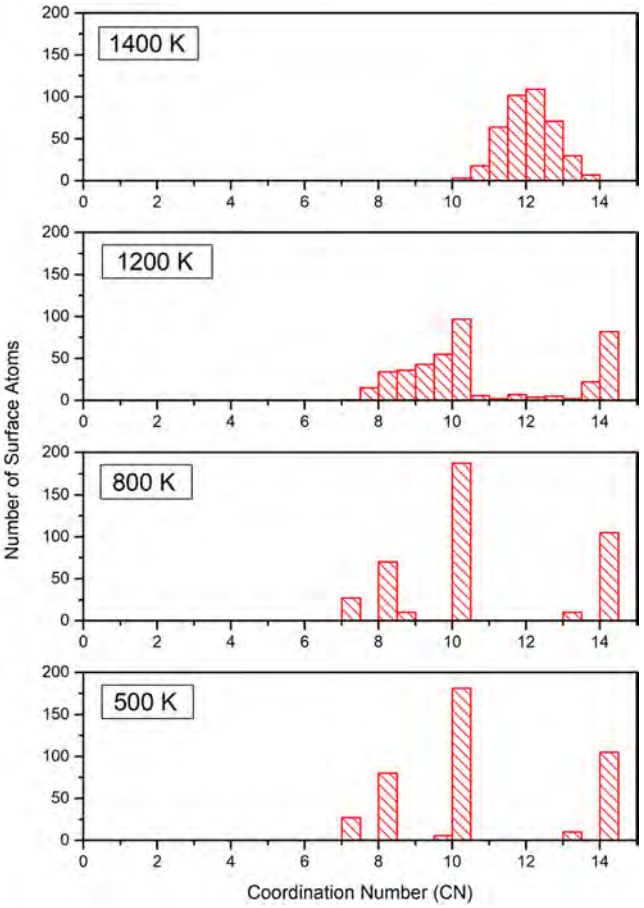

Figure 8. A histogram of the coordination numbers (CN) of the surface atoms on the 3 nm Fe_{1075} nanoparticle at different temperatures.

causes frequent exchange of atoms between the surface and the core. The surface atom that we identify in the beginning of the MD simulation can become core atoms. Therefore, the SCN at 1400 K shows a uniform distribution centered around 12, typical for core atoms in a liquid state.

As a system approaches surface premelting, how different are the surface and core atoms in terms of local environment? In Figure 9, we compare the local radial distribution function of a surface atom (in the middle of the facet) and an atom in the core of the nanoparticle at 700 K. At this temperature, the surface atoms have already lost the sharp peak at 2.86 Å, which corresponds to the second nearest neighbors in a BCC lattice [the first peak is at $(\sqrt{3}/2)a$, and the second peak is at a, where a is the BCC cell parameter]. However, this peak remains for the core atom. When comparing Figure 9 with Figure 7, it seems that the surface atoms at 700 K (Figure 9, red curve) are characterized by radial distribution functions similar to that of the whole system at 1200 K (Figure 7, blue curve), where the peak at 2.86 disappears completely.

Surface Premelting of an Fe Nanoparticle and Its Potential Catalytic Activity: Electronic Structure. In addition to SCN, the catalytic activity of the nanoparticle is also closely related to its electronic structure.[87] Figure 10 shows how the temperature affects the density of states (DOS) and d-band center of the nanoparticle, at the density functional tight-binding (DFTB) level of theory. Our calculations ignore potential magnetism in the nanoparticles; this is left for future

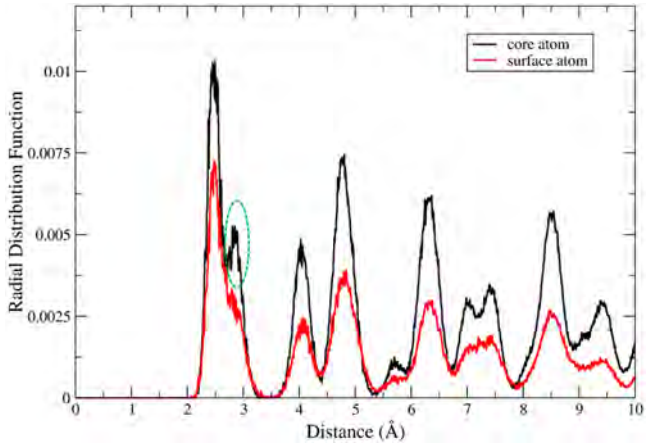

Figure 9. Radial distribution function of a surface atom in the middle of a (110) facet and an atom in the core of the Fe nanoparticle at 700 K.

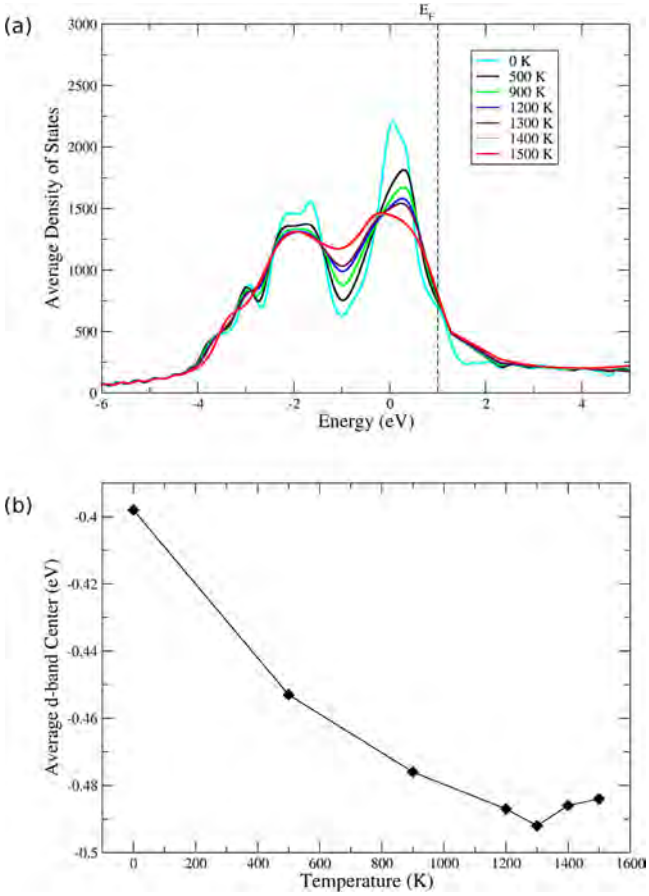

Figure 10. (a) The density of states and (b) d-band center of the 3 nm Fe_{1075} nanoparticle at all temperatures, with Fermi level as the reference (0 eV).

work. The calculation is averaged over 100 snapshots, which were picked out every 10000 steps from an MD trajectory of 1 ns. In Figure 10a, the 3 nm Fe nanoparticle definitely shows metallic character with high DOS at the Fermi level. When the temperature increases, the DOS at the Fermi level drops substantially, while the number of states increases in the region near −1.0 eV. The most obvious change happens in the following three regions: from 0 to 900 K, from 900 to 1200 K

DOI: 10.1021/acscatal.7b04468
ACS Catal. 2018, 8, 3365−3375

(surface premelting), and 1300 to 1400 K (melting region). The first region corresponds to increasing distortion of the structure from the local minimum energy by the vibrational motions. The second and third regions correspond to partial and full collapse of the crystalline structure of the NP, after passing the surface premelting point and the melting point, respectively. The "equalization" of the DOS is a structural effect caused by the increase of temperature. At low temperature, the atoms remain in crystalline positions. Because of the high translational symmetry, many of the electronic states are degenerate or close in energy, thereby forming sharp peaks on the DOS plot. However, when the temperature is increased, the displacement of the atoms breaks the symmetry of the underlying translational lattice. Therefore, the peaks on DOS plot begin to flatten out. The equalization of the DOS converges at 1400 K, after the nanoparticle is melted.

According to the d-band theory of catalysis,[88] the catalytic activity of a nanoparticle can be directly related to its d-band center.[89,90] As Figure 10b shows, the average d-band center of the Fe nanoparticle generally moves further away from the Fermi level as the temperature increases. It also converges at about 1400 K.

Melting and Surface Premelting Temperatures of Other Transition Metal Nanoparticles. As discussed in detail for the 3 nm Fe nanoparticle example, surface premelting has many important implications in catalysis. It is therefore interesting to know at what temperature the commonly used transition metal nanoparticles may premelt. From Figure 11, we

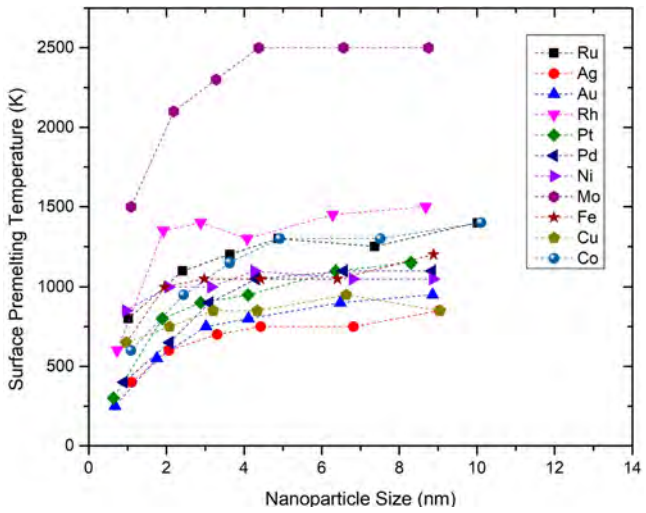

Figure 11. Surface premelting temperature of transition metal nanoparticles as a function of nanoparticle size.

can clearly see that an Au nanoparticle of very small size, say 1 and 2 nm, undergoes surface premelting at 250 and 550 K, respectively. Our results nicely explain the dynamic formation of Au single-atom active sites during the carbon monoxide oxidation reaction at 700 K reported by Li et al.[39] At the working temperature, some of the surface atoms of the Au nanoparticle melted ($\delta_i > 0.1$). Because of the greater degrees of freedom of these surface atoms, the in situ dynamic formation of a single-atom active site on the Au_{20} nanoparticle becomes possible, which one believes is responsible for its high catalytic activity in oxidation of carbon monoxide.

Our result is also in agreement with the experimental observation of the dynamic evolution of small Au clusters at room temperature (300 K)[91] and the formation of partially melted atomic regions on the surface of Au_{20} nanoparticles from AIMD simulations.[40] Other "soft" transition metal nanoparticles worthy of attention for exhibiting surface premelting at low temperature (300−700 K) are Pt, Pd, and Ag. The case of Ag is consistent with the experimental finding of liquidlike pseudoelasticity of sub-10 nm crystalline silver nanoparticles.[92] However, most of the other metals which form nanoparticles have surface activation temperature above 700 K. For these transition metal nanoparticles, surface premelting may happen in high temperature catalytic processes such as methane steam reforming.

CONCLUSIONS

To understand the surface activation of metallic nanoparticles in heterogeneous catalysis due to surface premelting, a systematic MD study of the premelting of 11 transition metal nanoparticles 1 to 8 nm in size is undertaken. Detailed discussions focus on a 3 nm Fe_{1075} nanoparticle. The overall Lindemann index is a good indication of the melting phenomenon and is a more sensitive indicator than the internal energy. The Lindemann index of the atoms indicates a temperature of surface activation that is consistent with thermodynamic predictions based on the equilibrium constant. More importantly, this index also identifies the atoms with high degrees of freedom (activated surface atom) during surface premelting. Due to the small size of a nanoparticle, the identity of the active atoms on a nanoparticle can change dynamically with time. A surface premelting temperature can be hundreds of Kelvin lower than the melting temperature of the nanoparticle, depending on the particle size.

Surface premelting not only causes the dynamic formation of active sites but generally affects three key factors related to catalysis: the surface coordination number, density of states, and d-band center of the nanoparticles on which potential catalysis may take place. The evolution of these characteristics is complex but can be understood. Surface premelting causes the atoms with high Lindemann index, usually located on the edges or vertices, to gain much greater kinetic energy than others. These atoms could potentially form new active sites in situ. When the temperature passes the surface premelting temperature, a drastic change in the coordination number of the surface atoms occurs, with dramatic broadening of the distribution of the SCN. The DOS of a nanoparticle tends to "equalize", due to the broken translational symmetry of the atoms in the nanoparticle. Also, the d-band center of the nanoparticle moves further away from the Fermi level as the temperature increases. Besides temperature, there are other factors that may affect the in situ formation of active sites in realistic conditions, such as pressure, coverage, and reactants; attention should also be paid to these.

We also show that the dynamic formation of active sites is not limited to Au nanoparticles. In fact, several noble transition metals that have fairly low surface premelting temperatures, such as Ag, Pt, and Pd, may also feature dynamic formation of unique active sites during catalytic reactions. Most of the other non-noble transition metals require a temperature of over 700 K for surface premelting to occur. We hope that our work may inspire the discovery and design of new nanocatalysts with in situ-formed unique active sites.

DOI: 10.1021/acscatal.7b04468
ACS Catal. 2018, 8, 3365−3375

■ ASSOCIATED CONTENT

Supporting Information

The Supporting Information is available free of charge on the ACS Publications website at DOI: 10.1021/acscatal.7b04468.

Unpublished surface energy of Ru from DFT calculations used for the Wulff construction of Ru nanoparticles, the number of atoms and sizes of all the nanoparticles studied, and the atomically resolved Lindemann index of all the nanoparticles at various temperatures (PDF)

■ AUTHOR INFORMATION

Corresponding Authors

*E-mail: wxd@sxicc.ac.cn.
*E-mail: rh34@cornell.edu.

ORCID

Xiaodong Wen: 0000-0001-5626-8581
Roald Hoffmann: 0000-0001-5369-6046

Author Contributions

The manuscript was written through contributions of all authors. All authors have given approval to the final version of the manuscript.

Notes

The authors declare no competing financial interest.

■ ACKNOWLEDGMENTS

The authors are grateful for the financial support from the National Natural Science Foundation of China (21603252, 21473229, 91545121), the Shanxi Province Science Foundation for Youth (201601D021048), and Synfuels China, Co. Ltd. We also acknowledge National Thousand Young Talents Program of China, Hundred-Talent Program of Chinese Academy of Sciences and Shanxi Hundred-Talent Program. The authors also would like to thank Prof. Dennis Salahub at the University of Calgary for helpful discussions. The comments of a reviewer were extraordinarily useful to the authors, as they pointed us to literature that we had missed; we are grateful for this help. The computational resources for the project were supplied by the Tianhe-2 in Lvliang, Shanxi, People's Republic of China.

■ ABBREVIATIONS

CN, coordination number; RDF, radial distribution function; DOS, density of states

■ REFERENCES

(1) Hansen, K., Melting and Freezing. In *Statistical Physics of Nanoparticles in the Gas Phase*, 1st ed.; Springer: Dordrecht, The Netherlands, 2013; Vol. 73, pp 247−262.
(2) Bachels, T.; Güntherodt, H.-J.; Schäfer, R. Melting of Isolated Tin Nanoparticles. *Phys. Rev. Lett.* **2000**, *85*, 1250−1253.
(3) Alavi, S.; Thompson, D. L. Molecular Dynamics Simulations of the Melting of Aluminum Nanoparticles. *J. Phys. Chem. A* **2006**, *110*, 1518−1523.
(4) Stephen Berry, R.; Beck, T. L.; Davis, H. L.; Jellinek, J. Solid-Liquid Phase Behavior in Microclusters. In *Advances in Chemical Physics*, 1st ed.; John Wiley & Sons, Inc., 2007; Vol. 70, pp 75−138.
(5) Losurdo, M.; Suvorova, A.; Rubanov, S.; Hingerl, K.; Brown, A. S. Thermally Stable Coexistence of Liquid and Solid Phases in Gallium Nanoparticles. *Nat. Mater.* **2016**, *15*, 995−1002.
(6) Aguado, A. Nanoparticles: Neither Solid nor Liquid. *Nat. Mater.* **2016**, *15*, 931−933.
(7) Lai, S. L.; Guo, J. Y.; Petrova, V.; Ramanath, G.; Allen, L. H. Size-Dependent Melting Properties of Small Tin Particles: Nanocalorimetric Measurements. *Phys. Rev. Lett.* **1996**, *77*, 99−102.
(8) Peters, K. F.; Cohen, J. B.; Chung, Y.-W. Melting of Pb Nanocrystals. *Phys. Rev. B: Condens. Matter Mater. Phys.* **1998**, *57*, 13430−13438.
(9) Wang, Z. L.; Petroski, J. M.; Green, T. C.; El-Sayed, M. A. Shape Transformation and Surface Melting of Cubic and Tetrahedral Platinum Nanocrystals. *J. Phys. Chem. B* **1998**, *102*, 6145−6151.
(10) de Heer, W. A. The Physics of Simple Metal Clusters: Experimental Aspects and Simple Models. *Rev. Mod. Phys.* **1993**, *65*, 611−676.
(11) Kirkland, A. I.; Edwards, P. P.; Jefferson, D. A.; Duff, D. G. Chapter 8. The Structure, Characterization, and Evolution of Colloidal Metals. *Annu. Rep. Prog. Chem., Sect. C: Phys. Chem.* **1990**, *87*, 247−304.
(12) Penn, R. L.; Banfield, J. F. Imperfect Oriented Attachment: Dislocation Generation in Defect-Free Nanocrystals. *Science* **1998**, *281*, 969−971.
(13) McKenna, K. P.; Sushko, P. V.; Shluger, A. L. Transient Atomic Configurations of Supported Gold Nanocrystallites at Finite Temperature. *J. Phys. Chem. C* **2007**, *111*, 2823−2826.
(14) Risse, T.; Mozaffari-Afshar, M.; Hamann, H.; Freund, H.-J. Structural Changes in Nanoparticle Catalysts as Monitored by Their Magnetic Properties. *Angew. Chem., Int. Ed.* **2004**, *43*, 517−520.
(15) Frenkel, A. I.; Hills, C. W.; Nuzzo, R. G. A View from the Inside: Complexity in the Atomic Scale Ordering of Supported Metal Nanoparticles. *J. Phys. Chem. B* **2001**, *105*, 12689−12703.
(16) Müller, P.; Saúl, A. Elastic Effects on Surface Physics. *Surf. Sci. Rep.* **2004**, *54*, 157−258.
(17) Mayoral, A.; Barron, H.; Estrada-Salas, R.; Vazquez-Duran, A.; Jose-Yacaman, M. Nanoparticle Stability from the Nano to the Meso Interval. *Nanoscale* **2010**, *2*, 335−342.
(18) Baumgardner, W. J.; Yu, Y.; Hovden, R.; Honrao, S.; Hennig, R. G.; Abruña, H. D.; Muller, D.; Hanrath, T. Nanoparticle Metamorphosis: An in Situ High-Temperature Transmission Electron Microscopy Study of the Structural Evolution of Heterogeneous Au:Fe_2O_3 Nanoparticles. *ACS Nano* **2014**, *8*, 5315−5322.
(19) Ajayan, P. M.; Marks, L. D. Quasimelting and Phases of Small Particles. *Phys. Rev. Lett.* **1988**, *60*, 585−587.
(20) Sakai, H. How Does a Slab-Shaped Solid Melt? *Surf. Sci.* **1996**, *348*, 387−392.
(21) Sun, C. Q. Size Dependence of Nanostructures: Impact of Bond Order Deficiency. *Prog. Solid State Chem.* **2007**, *35*, 1−159.
(22) Sayle, D. C.; Watson, G. W. The Atomistic Structure of an MgO Cluster, Supported on BaO, Synthesized Using Simulated Amorphization and Recrystallization. *J. Phys. Chem. B* **2002**, *106*, 3916−3925.
(23) Sayle, T. X. T.; Catlow, C. R. A.; Maphanga, R. R.; Ngoepe, P. E.; Sayle, D. C. Generating MnO_2 Nanoparticles Using Simulated Amorphization and Recrystallization. *J. Am. Chem. Soc.* **2005**, *127*, 12828−12837.
(24) Qi, Y.; Cagin, T.; Johnson, W. L.; Goddard, W. A. Melting and Crystallization in Ni Nanoclusters: The Mesoscale Regime. *J. Chem. Phys.* **2001**, *115*, 385−394.
(25) Chushak, Y. G.; Bartell, L. S. Melting and Freezing of Gold Nanoclusters. *J. Phys. Chem. B* **2001**, *105*, 11605−11614.
(26) Vanfleet, R. R.; Mochel, J. M. Thermodynamics of Melting and Freezing in Small Particles. *Surf. Sci.* **1995**, *341*, 40−50.
(27) Lewis, L. J.; Jensen, P.; Barrat, J. L. Melting, Freezing, and Coalescence of Gold Nanoclusters. *Phys. Rev. B: Condens. Matter Mater. Phys.* **1997**, *56*, 2248−2257.
(28) Chui, Y. H.; Snook, I. K.; Russo, S. P. Visualization and Analysis of Structural Ordering During Crystallization of a Gold Nanoparticle. *Phys. Rev. B: Condens. Matter Mater. Phys.* **2007**, *76*, 195427.
(29) Barnard, A. S.; Chen, Y. Kinetic Modelling of the Shape-Dependent Evolution of Faceted Gold Nanoparticles. *J. Mater. Chem.* **2011**, *21*, 12239−12245.

DOI: 10.1021/acscatal.7b04468
ACS Catal. 2018, 8, 3365−3375

(30) Doye, J. P. K.; Calvo, F. Entropic Effects on the Size Dependence of Cluster Structure. *Phys. Rev. Lett.* **2001**, *86*, 3570−3573.
(31) Baletto, F.; Ferrando, R. Structural Properties of Nanoclusters: Energetic, Thermodynamic, and Kinetic Effects. *Rev. Mod. Phys.* **2005**, *77*, 371−423.
(32) Barnard, A. S. Modelling of Nanoparticles: Approaches to Morphology and Evolution. *Rep. Prog. Phys.* **2010**, *73*, 086502.
(33) Marks, L. D.; Peng, L. Nanoparticle Shape, Thermodynamics and Kinetics. *J. Phys.: Condens. Matter* **2016**, *28*, 053001.
(34) Vajda, S.; Lee, S.; Sell, K.; Barke, I.; Kleibert, A.; von Oeynhausen, V.; Meiwes-Broer, K.-H.; Rodríguez, A. F.; Elam, J. W.; Pellin, M. M.; Lee, B.; Seifert, S.; Winans, R. E. Combined Temperature-Programmed Reaction and in Situ X-Ray Scattering Studies of Size-Selected Silver Clusters under Realistic Reaction Conditions in the Epoxidation of Propene. *J. Chem. Phys.* **2009**, *131*, 121104.
(35) Zhang, X.-Q.; Iype, E.; Nedea, S. V.; Jansen, A. P. J.; Szyja, B. M.; Hensen, E. J. M.; van Santen, R. A. Site Stability on Cobalt Nanoparticles: A Molecular Dynamics ReaxFF Reactive Force Field Study. *J. Phys. Chem. C* **2014**, *118*, 6882−6886.
(36) Krstajić Pajić, M. N.; Stevanović, S. I.; Radmilović, V. V.; Gavrilović-Wohlmuther, A.; Radmilović, V. R.; Gojković, S. L.; Jovanović, V. M. Shape Evolution of Carbon Supported Pt Nanoparticles: From Synthesis to Application. *Appl. Catal., B* **2016**, *196*, 174−184.
(37) Matam, S. K.; Kondratenko, E. V.; Aguirre, M. H.; Hug, P.; Rentsch, D.; Winkler, A.; Weidenkaff, A.; Ferri, D. The Impact of Aging Environment on the Evolution of Al_2O_3 Supported Pt Nanoparticles and Their NO Oxidation Activity. *Appl. Catal., B* **2013**, *129*, 214−224.
(38) Barron, H.; Opletal, G.; Tilley, R. D.; Barnard, A. S. Dynamic Evolution of Specific Catalytic Sites on Pt Nanoparticles. *Catal. Sci. Technol.* **2016**, *6*, 144−151.
(39) Wang, Y.-G.; Mei, D.; Glezakou, V.-A.; Li, J.; Rousseau, R. Dynamic Formation of Single-Atom Catalytic Active Sites on Ceria-Supported Gold Nanoparticles. *Nat. Commun.* **2015**, *6*, 6511.
(40) Wang, Y.-G.; Yoon, Y.; Glezakou, V.-A.; Li, J.; Rousseau, R. The Role of Reducible Oxide−Metal Cluster Charge Transfer in Catalytic Processes: New Insights on the Catalytic Mechanism of CO Oxidation on Au/TiO_2 from Ab Initio Molecular Dynamics. *J. Am. Chem. Soc.* **2013**, *135*, 10673−10683.
(41) Wang, Y.-G.; Cantu, D. C.; Lee, M.-S.; Li, J.; Glezakou, V.-A.; Rousseau, R. CO Oxidation on Au/TiO_2: Condition-Dependent Active Sites and Mechanistic Pathways. *J. Am. Chem. Soc.* **2016**, *138*, 10467−10476.
(42) Lebarbier, V. M.; Mei, D.; Kim, D. H.; Andersen, A.; Male, J. L.; Holladay, J. E.; Rousseau, R.; Wang, Y. Effects of La_2O_3 on the Mixed Higher Alcohols Synthesis from Syngas over Co Catalysts: A Combined Theoretical and Experimental Study. *J. Phys. Chem. C* **2011**, *115*, 17440−17451.
(43) Mei, D.; Glezakou, V.-A.; Lebarbier, V.; Kovarik, L.; Wan, H.; Albrecht, K. O.; Gerber, M.; Rousseau, R.; Dagle, R. A. Highly Active and Stable $MgAl_2O_4$-Supported Rh and Ir Catalysts for Methane Steam Reforming: A Combined Experimental and Theoretical Study. *J. Catal.* **2014**, *316*, 11−23.
(44) Hansen, P. L.; Wagner, J. B.; Helveg, S.; Rostrup-Nielsen, J. R.; Clausen, B. S.; Topsøe, H. Atom-Resolved Imaging of Dynamic Shape Changes in Supported Copper Nanocrystals. *Science* **2002**, *295*, 2053−2055.
(45) Tyrsted, C.; Ørnsbjerg Jensen, K. M.; Bøjesen, E. D.; Lock, N.; Christensen, M.; Billinge, S. J. L.; Brummerstedt Iversen, B. Understanding the Formation and Evolution of Ceria Nanoparticles under Hydrothermal Conditions. *Angew. Chem., Int. Ed.* **2012**, *51*, 9030−9033.
(46) Tyrsted, C.; Pauw, B. R.; Jensen, K. M. Ø.; Becker, J.; Christensen, M.; Iversen, B. B. Watching Nanoparticles Form: An in Situ (Small-/Wide-Angle X-Ray Scattering/Total Scattering) Study of the Growth of Yttria-Stabilised Zirconia in Supercritical Fluids. *Chem. - Eur. J.* **2012**, *18*, 5759−5766.
(47) Fredriksson, H. O. A.; Larsson Langhammer, E. M.; Niemantsverdriet, J. W. Reduction of Cu-Promoted Fe Model Catalysts Studied by in Situ Indirect Nanoplasmonic Sensing and X-Ray Photoelectron Spectroscopy. *J. Phys. Chem. C* **2015**, *119*, 4085−4094.
(48) Saha, D.; Jensen, K. M. Ø.; Tyrsted, C.; Bøjesen, E. D.; Mamakhel, A. H.; Dippel, A.-C.; Christensen, M.; Iversen, B. B. In Situ Total X-Ray Scattering Study of WO_3 Nanoparticle Formation under Hydrothermal Conditions. *Angew. Chem., Int. Ed.* **2014**, *53*, 3667−3670.
(49) Dann, E. K.; Gibson, E. K.; Catlow, R. A.; Collier, P.; Eralp Erden, T.; Gianolio, D.; Hardacre, C.; Kroner, A.; Raj, A.; Goguet, A.; Wells, P. P. Combined in Situ XAFS/DRIFTS Studies of the Evolution of Nanoparticle Structures from Molecular Precursors. *Chem. Mater.* **2017**, *29*, 7515−7523.
(50) Zou, L.; Li, J.; Zakharov, D.; Stach, E. A.; Zhou, G. In Situ Atomic-Scale Imaging of the Metal/Oxide Interfacial Transformation. *Nat. Commun.* **2017**, *8*, 307.
(51) Kalz, K. F.; Kraehnert, R.; Dvoyashkin, M.; Dittmeyer, R.; Gläser, R.; Krewer, U.; Reuter, K.; Grunwaldt, J.-D. Future Challenges in Heterogeneous Catalysis: Understanding Catalysts under Dynamic Reaction Conditions. *ChemCatChem* **2017**, *9*, 17−29.
(52) Tang, P.; Zhu, Q.; Wu, Z.; Ma, D. Methane Activation: The Past and Future. *Energy Environ. Sci.* **2014**, *7*, 2580−2591.
(53) Sadykov, V. A.; Isupova, L. A.; Zolotarskii, I. A.; Bobrova, L. N.; Noskov, A. S.; Parmon, V. N.; Brushtein, E. A.; Telyatnikova, T. V.; Chernyshev, V. I.; Lunin, V. V. Oxide Catalysts for Ammonia Oxidation in Nitric Acid Production: Properties and Perspectives. *Appl. Catal., A* **2000**, *204*, 59−87.
(54) Steele, B. C. H.; Heinzel, A. Materials for Fuel-Cell Technologies. *Nature* **2001**, *414*, 345−352.
(55) Wirth, C. T.; Bayer, B. C.; Gamalski, A. D.; Esconjauregui, S.; Weatherup, R. S.; Ducati, C.; Baehtz, C.; Robertson, J.; Hofmann, S. The Phase of Iron Catalyst Nanoparticles During Carbon Nanotube Growth. *Chem. Mater.* **2012**, *24*, 4633−4640.
(56) Suárez, M. P.; Löffler, D. G. Hcn Synthesis from NH_3 and CH_4 on Pt at Atmospheric Pressure. *J. Catal.* **1986**, *97*, 240−242.
(57) Zhu, L. *Surface Temperature Excess in Heterogeneous Catalysis*; Delft University of Technology: The Netherlands, 2005.
(58) Taccardi, N.; Grabau, M.; Debuschewitz, J.; Distaso, M.; Brandl, M.; Hock, R.; Maier, F.; Papp, C.; Erhard, J.; Neiss, C.; Peukert, W.; Görling, A.; Steinrück, H. P.; Wasserscheid, P. Gallium-Rich Pd−Ga Phases as Supported Liquid Metal Catalysts. *Nat. Chem.* **2017**, *9*, 862−867.
(59) Ding, F.; Bolton, K.; Rosén, A. Molecular Dynamics Study of the Surface Melting of Iron Clusters. *Eur. Phys. J. D* **2005**, *34*, 275−277.
(60) Engelmann, Y.; Bogaerts, A.; Neyts, E. C. Thermodynamics at the Nanoscale: Phase Diagrams of Nickel-Carbon Nanoclusters and Equilibrium Constants for Phase Transitions. *Nanoscale* **2014**, *6*, 11981−11987.
(61) Özdoğan, C.; Erkoç, Ş. Molecular-Dynamics Simulation of the Structural Stability, Energetics, and Melting of Cu_n (n = 13−135) Clusters. *Z. Phys. D: At., Mol. Clusters* **1997**, *41*, 205−209.
(62) Alarifi, H. A.; Atiş, M.; Özdoğan, C.; Hu, A.; Yavuz, M.; Zhou, Y. Determination of Complete Melting and Surface Premelting Points of Silver Nanoparticles by Molecular Dynamics Simulation. *J. Phys. Chem. C* **2013**, *117*, 12289−12298.
(63) Akbarzadeh, H.; Yaghoubi, H. Molecular Dynamics Simulations of Silver Nanocluster Supported on Carbon Nanotube. *J. Colloid Interface Sci.* **2014**, *418*, 178−184.
(64) Li, S.; Qi, W.; Peng, H.; Wu, J. A Comparative Study on Melting of Core−Shell and Janus Cu−Ag Bimetallic Nanoparticles. *Comput. Mater. Sci.* **2015**, *99*, 125−132.
(65) Hoffmann, H. J. On Lindemann's Melting Criterion. *Materialwiss. Werkstofftech.* **2004**, *35*, 79−81.

DOI: 10.1021/acscatal.7b04468
ACS Catal. 2018, 8, 3365−3375

(66) Calvo, F.; Spiegelmann, F. Mechanisms of Phase Transitions in Sodium Clusters: From Molecular to Bulk Behavior. *J. Chem. Phys.* **2000**, *112*, 2888−2908.
(67) Susan, A.; Kibey, A.; Kaware, V.; Joshi, K. Correlation between the Variation in Observed Melting Temperatures and Structural Motifs of the Global Minima of Gallium Clusters: An Ab Initio Study. *J. Chem. Phys.* **2013**, *138*, 014303.
(68) Chernyshev, A. P. Effect of Nanoparticle Size on the Onset Temperature of Surface Melting. *Mater. Lett.* **2009**, *63*, 1525−1527.
(69) Wulff, G. Zur Frage der Geschwindigkeit des Wachsturms under Auflösung der Kristallflächen. *Z. Kristallogr. - Cryst. Mater.* **1901**, *34*, 449−530.
(70) Wen, Y.-N.; Zhang, J.-M. Surface Energy Calculation of the BCC Metals by Using the Maeam. *Comput. Mater. Sci.* **2008**, *42*, 281−285.
(71) Wen, Y.-N.; Zhang, J.-M. Surface Energy Calculation of the FCC Metals by Using the Maeam. *Solid State Commun.* **2007**, *144*, 163−167.
(72) Vitos, L.; Ruban, A. V.; Skriver, H. L.; Kollár, J. The Surface Energy of Metals. *Surf. Sci.* **1998**, *411*, 186−202.
(73) Foiles, S. M.; Baskes, M. I.; Daw, M. S. Embedded-Atom-Method Functions for the FCC Metals Cu, Ag, Au, Ni, Pd, Pt, and Their Alloys. *Phys. Rev. B: Condens. Matter Mater. Phys.* **1986**, *33*, 7983−7991.
(74) Pun, G. P. P.; Mishin, Y. Embedded-Atom Potential for HCP and FCC Cobalt. *Phys. Rev. B: Condens. Matter Mater. Phys.* **2012**, *86*, 134116.
(75) Mendelev, M. I.; Han, S.; Srolovitz, D. J.; Ackland, G. J.; Sun, D. Y.; Asta, M. Development of New Interatomic Potentials Appropriate for Crystalline and Liquid Iron. *Philos. Mag.* **2003**, *83*, 3977−3994.
(76) Fortini, A.; Mendelev, M. I.; Buldyrev, S.; Srolovitz, D. Asperity Contacts at the Nanoscale: Comparison of Ru and Au. *J. Appl. Phys.* **2008**, *104*, 074320.
(77) Sheng, H. W.; Kramer, M. J.; Cadien, A.; Fujita, T.; Chen, M. W. Highly Optimized Embedded-Atom-Method Potentials for Fourteen FCC Metals. *Phys. Rev. B: Condens. Matter Mater. Phys.* **2011**, *83*, 134118.
(78) Wang, Y.; Dellago, C. Structural and Morphological Transitions in Gold Nanorods: A Computer Simulation Study. *J. Phys. Chem. B* **2003**, *107*, 9214−9219.
(79) Link, S.; Wang, Z. L.; El-Sayed, M. A. How Does a Gold Nanorod Melt? *J. Phys. Chem. B* **2000**, *104*, 7867−7870.
(80) Ackland, G. J.; Thetford, R. An Improved N-Body Semi-Empirical Model for Body-Centred Cubic Transition Metals. *Philos. Mag. A* **1987**, *56*, 15−30.
(81) Aradi, B.; Hourahine, B.; Frauenheim, T. DFTB+, a Sparse Matrix-Based Implementation of the DFTB Method. *J. Phys. Chem. A* **2007**, *111*, 5678−5684.
(82) Kohler, C.; Seifert, G.; Frauenheim, T. Density Functional Based Calculations for Fe_n ($n \leq 32$). *Chem. Phys.* **2005**, *309*, 23−31.
(83) Zambelli, T.; Wintterlin, J.; Trost, J.; Ertl, G. Identification of the "Active Sites" of a Surface-Catalyzed Reaction. *Science* **1996**, *273*, 1688−1690.
(84) Calle-Vallejo, F.; Tymoczko, J.; Colic, V.; Vu, Q. U.; Pohl, M. D.; Morgenstern, K.; Loffreda, D.; Sautet, P.; Schuhmann, W.; Bandarenka, A. S. Finding Optimal Surface Sites on Heterogeneous Catalysts by Counting Nearest Neighbors. *Science* **2015**, *350*, 185−189.
(85) Mikolaj, P. G.; Pings, C. J. The Use of the Coordination Number in the Interpretation of Fluid Structure. *Phys. Chem. Liq.* **1968**, *1*, 93−108.
(86) Wen, X.-D.; Cahill, T. J.; Hoffmann, R. Exploring Group 14 Structures: 1d to 2d to 3d. *Chem. - Eur. J.* **2010**, *16*, 6555−6566.
(87) Norskov, J. K.; Bligaard, T.; Rossmeisl, J.; Christensen, C. H. Towards the Computational Design of Solid Catalysts. *Nat. Chem.* **2009**, *1*, 37−46.
(88) Nilsson, A.; Pettersson, L. G. M.; Hammer, B.; Bligaard, T.; Christensen, C. H.; Norskov, J. K. The Electronic Structure Effect in Heterogeneous Catalysis. *Catal. Lett.* **2005**, *100*, 111−114.
(89) Crampton, A. S.; Rotzer, M. D.; Schweinberger, F. F.; Yoon, B.; Landman, U.; Heiz, U. Ethylene Hydrogenation on Supported Ni, Pd and Pt Nanoparticles: Catalyst Activity, Deactivation and the D-Band Model. *J. Catal.* **2016**, *333*, 51−58.
(90) Toyoda, E.; Jinnouchi, R.; Hatanaka, T.; Morimoto, Y.; Mitsuhara, K.; Visikovskiy, A.; Kido, Y. The d-Band Structure of Pt Nanoclusters Correlated with the Catalytic Activity for an Oxygen Reduction Reaction. *J. Phys. Chem. C* **2011**, *115*, 21236−21240.
(91) Li, Z. Y.; Young, N. P.; Di Vece, M.; Palomba, S.; Palmer, R. E.; Bleloch, A. L.; Curley, B. C.; Johnston, R. L.; Jiang, J.; Yuan, J. Three-Dimensional Atomic-Scale Structure of Size-Selected Gold Nanoclusters. *Nature* **2008**, *451*, 46−48.
(92) Sun, J.; He, L.; Lo, Y.-C.; Xu, T.; Bi, H.; Sun, L.; Zhang, Z.; Mao, S. X.; Li, J. Liquid-Like Pseudoelasticity of Sub-10-nm Crystalline Silver Particles. *Nat. Mater.* **2014**, *13*, 1007−1012.

DOI: 10.1021/acscatal.7b04468
ACS Catal. 2018, 8, 3365−3375